



1 **Radionuclide wiggle-matching reveals a non-synchronous**
2 **Early Holocene climate oscillation in Greenland and Western**
3 **Europe around a grand solar minimum**

4

5 Florian Mekhaldi¹, Markus Czymzik², Florian Adolphi^{1,3}, Jesper Sjolte¹, Svante Björck¹, Ala
6 Aldahan⁴, Achim Brauer⁵, Celia Martin-Puertas⁶, Göran Possnert⁷, and Raimund Muscheler¹

7

8 ¹Department of Geology - Quaternary Sciences, Lund University, 22362Lund, Sweden

9 ²Leibniz-Institute for Baltic Sea Research Warnemünde (IOW), Marine Geology, 18119 Rostock, Germany

10 ³Physics Institute, Climate and Environmental Physics & Oeschger Centre for Climate Change Research,
11 University of Bern, 3012 Bern, Switzerland

12 ⁴Department of Geology, United Arab Emirates University, 15551 Al Ain, UAE

13 ⁵GFZ-German Research Centre for Geosciences, Climate Dynamics and Landscape Evolution, 14473 Potsdam,
14 Germany

15 ⁶Department of Geography, Royal Holloway University of London, Egham, Surrey TW20 0EX, UK

16 ⁷Tandem Laboratory, Uppsala University, 75120 Uppsala, Sweden

17

18 *Correspondence to:* Florian Mekhaldi (florian.mekhaldi@geol.lu.se)

19

20

21 **Abstract.** Several climate events have been reported from the Early Holocene superepoch, the best known of these
22 being the Preboreal oscillation (PBO). It is still unclear how the PBO and the number of climate events observed
23 in Greenland ice cores and European terrestrial records are related to one another. This is mainly due to
24 uncertainties in the chronologies of the records. Here, we present new high resolution ¹⁰Be concentration data from
25 the varved Meerfelder Maar sediment record in Germany, spanning the period 11,310-11,000 years BP. These
26 new data allow us to synchronize this well-studied record as well as Greenland ice-core records to the IntCal13
27 time-scale via radionuclide wiggle-matching. In doing so, we show that the climate oscillations identified in
28 Greenland and Europe between 11,450 and 11,000 years BP were not synchronous but terminated and began,
29 respectively, with the onset of a grand solar minimum. A similar spatial anomaly pattern is found in a number of
30 modeling studies on solar forcing of climate in the North Atlantic region. We further postulate that freshwater
31 delivery to the North Atlantic would have had the potential to amplify solar forcing through a slowdown of the
32 Atlantic meridional overturning circulation (AMOC) reinforcing surface air temperature anomalies in the region.

33

34

35

36

37

38

39

40



41 1 Introduction

42 One of the great challenges in paleoclimatology today is to better assess the spatial and temporal dynamics of past
43 climate changes. This can only be achieved through robust and consistent chronologies for different records and
44 different regions. Unfortunately, this is a challenging task and we often assume synchrony of such events by
45 climate-tuning different records. One such example is the Preboreal oscillation (PBO) (Björck et al., 1996) and
46 represents a cold spell which occurred shortly after the Younger-Dryas/Holocene transition. Indications of a cold
47 phase have also been reported in a number of European terrestrial records, most of which use biological proxy and
48 isotope data (Björck et al., 1996; Björck et al., 1997; Bos et al., 2007; Magny et al., 2007, van der Plicht et al.,
49 2004; von Grafenstein et al., 1999). A cold and dry climate oscillation, thought to be related to the European PBO,
50 has also been observed in the $\delta^{18}\text{O}$ and accumulation signals of a number of Greenland ice cores between 11,520-
51 11,400 years before AD 2000 (b2k) and referred to as the 11.4 ka event (Rasmussen et al., 2007; 2014). Due to
52 chronology uncertainties, it is however unclear whether the 11.4 ka event in Greenland and the European PBO
53 represent one single and synchronous widespread event, an event that spread over time, or whether the European
54 PBO is unrelated to the 11.4 ka event in Greenland. These open questions limit our understanding of the underlying
55 mechanisms of these climate changes.

56 Around this period, one of the largest and the longest-lasting grand minimum in solar activity of the
57 Holocene occurred between 11,280-10,960 years before AD 1950 (BP). This was evidenced by beryllium-10
58 (^{10}Be) data in the GISP2 and GRIP ice cores in central Greenland (Finkel and Nishiizumi, 1997; Muscheler et al.,
59 2004; Adolphi et al., 2014) and by $\Delta^{14}\text{C}$ ($^{14}\text{C}/^{12}\text{C}$ corrected for fractionation and decay, relative to a standard, and
60 noted as Δ in Stuiver and Polach (1977)) derived from tree rings (Reimer et al., 2013). This substantial change in
61 solar activity (from high to persistently low) offers an advantage to us for synchronizing time-scales as it has left
62 a clear imprint on the atmospheric production rate of the cosmogenic radionuclides ^{10}Be and ^{14}C . That is, these
63 radionuclides are produced by a nuclear cascade that is triggered when cosmic rays enter the atmosphere. The
64 Earth is shielded, to some extent, from these cosmic rays by the fluctuating strength of the helio- and geomagnetic
65 fields. Therefore, radionuclides carry in part the signal of solar activity, which is then stored in natural archives
66 such as in polar ice caps or lake sediments (^{10}Be) as well as in tree rings (^{14}C). In consequence, we can use these
67 global fluctuations in atmospheric production rate of radionuclides to synchronize records from different
68 environmental archives and investigate the timing of climate events during the earliest part of the Holocene
69 (Southon, 2002; Muscheler et al., 2014; Adolphi and Muscheler, 2016).

70 Here we present new high-resolution ^{10}Be concentration measurements from the well-studied varved
71 Meerfelder Maar sediment record (MFM) in western Germany, spanning across these large fluctuations in solar
72 activity from 11,310 to 11,000 years BP. Because of its limited catchment area and the existence of ^{10}Be data
73 covering the Late Glacial-Holocene transition (Czymzik et al., 2016), MFM represents an ideal location for the
74 aim of this study. As such, the new ^{10}Be data allow us to synchronize the MFM and Greenland ice core records
75 with the IntCal13 time-scale through wiggle-matching of these different radionuclide records. We can then
76 investigate the timing of the fluctuations observed in the corresponding paleoclimate records at a high
77 chronological precision and assess their relationship in regard to changes in solar activity.

78



79 2 Methods

80 2.1 Preparation of sediment ¹⁰Be samples

81 The new ¹⁰Be samples come from the composite sediment profile MFM09 (Martin-Puertas et al., 2012a) which
82 was retrieved at MFM, a deep crater lake situated in the Eifel region in western Germany that is annually
83 laminated (varved) throughout most of the Holocene (Brauer et al., 2000). About 0.25 g of dried and crushed
84 material was taken for each sample with a temporal resolution of 3 and 10 years (see dataset in Sup. Info.) and 0.5
85 mg of ⁹Be carrier was added. ¹⁰Be was extracted from the sediment samples at the ¹⁰Be laboratory of the Earth
86 Sciences Department of Uppsala University, Sweden, following the methodology described by Berggren et al.
87 (2010). All samples were measured using the Accelerator Mass Spectrometer (AMS) of the Tandem laboratory in
88 Uppsala. The ¹⁰Be concentration (in atoms/g) of each sample is calculated based on the ¹⁰Be counts *R* to ⁹Be counts
89 *R_{st}* ratio and taking in consideration the NIST SRM 4325 reference standard (¹⁰Be/⁹Be = 2.68 10⁻¹¹), the weights
90 of the carrier *W_C* and of the sample *W_S* as well as the Avogadro constant *N_A* and atomic weight *A_r* of beryllium:

$$91 \quad {}^{10}\text{Be conc.} = \frac{R}{R_{st}} * 2.68 \cdot 10^{-11} * \frac{W_C}{W_S} * \frac{N_A}{A_r}$$

92

93 2.2 Chronologies and synchronization

94 The paleoclimate data investigated henceforth come from different studies, with different records and thus
95 different chronologies. The new sediment ¹⁰Be concentration data come from MFM, the chronology of which
96 (MFM2012) was established using mainly microscopic varve counting fixed on an absolute time-scale via
97 tephrochronology as well as radiocarbon dating with a maximum varve counting error of up to 110 years (Brauer
98 et al., 2000; Martin-Puertas et al., 2012a). A more recent chronology (MFM2015) exists which includes the
99 identification and age of the Vedde Ash although it remains unchanged for the Holocene part (Lane et al., 2015),
100 which is the period of focus in this study. We also use published ¹⁰Be data (Adolphi et al., 2014) from the GRIP
101 ice core in central Greenland and within the Greenland Ice Core Chronology (GICC05) framework (Rasmussen et
102 al., 2006; Vinther et al., 2006; Svensson et al., 2008; Seierstad et al., 2014). Finally, we use ¹⁴C production rate
103 data (Muscheler et al., 2014) inferred from the IntCal13 ¹⁴C calibration curve (Reimer et al., 2013) as the anchoring
104 record for our synchronization. That is, we synchronize the MFM2012 time-scale (using our ¹⁰Be concentration
105 data) as well as the GICC05 time-scale (using the GRIP ¹⁰Be concentration data) to IntCal13 (using the ¹⁴C
106 production rate data).

107 The synchronization of the different radionuclide records was computed following the methodology
108 described by Adolphi and Muscheler (2016). For these calculations we linearly detrend all radionuclide records
109 between 11,000 and 11,800 years BP and assumed a production rate uncertainty of 20% for all records, which
110 corresponds to the root mean square error between the records after synchronization.

111

112

113



114 3 Results

115 3.1 Meerfelder Maar ^{10}Be concentrations

116 The new ^{10}Be concentration measurements from MFM are displayed in Fig. 1, alongside with ^{10}Be concentrations
117 from the GRIP ice core in central Greenland (Finkel and Nishiizumi, 1997; Muscheler et al., 2004; Adolphi et al.,
118 2014), and with older ^{10}Be concentration data from MFM for the Late Glacial-Holocene transition (Czymzik et
119 al., 2016). Each dataset is plotted on its original time-scale – that is, the MFM2012 chronology (Brauer et al.,
120 2000; Martin-Puertas et al., 2012a) and the GICC05 chronology (Rasmussen et al., 2006; Vinther et al., 2006;
121 Svensson et al., 2008; Seierstad et al., 2014). The most striking feature of these datasets is the approximately 250-
122 year long period of increased ^{10}Be concentration around 11,150 years BP. The most likely explanation for this
123 increase is a decrease in the intensity of the heliomagnetic field (solar activity) leading to an increased
124 impingement of Earth by galactic cosmic rays and thus, an increased atmospheric production rate of ^{10}Be and ^{14}C
125 nuclides. It was also shown that meteorological and catchment influences on ^{10}Be deposition are likely small at
126 MFM (Czymzik et al., 2016). The high resolution of our ^{10}Be measurements allows us to observe finer structures
127 within this period of increased ^{10}Be concentration. One example is the double peak structure at 11,040 and 11,200
128 years BP, which is also present in ^{14}C atmospheric production rate data (Muscheler et al., 2014), but not well-
129 expressed in the GRIP ^{10}Be data. Finally, it is of importance to note that although the increased production around
130 11,150 years BP is observed in all these radionuclide records, there is an apparent chronology offset at its onset
131 around 11,300 years BP (Fig. 1). More specifically, the ^{10}Be concentration data from GRIP begin to increase
132 around 11,320 years BP whereas a similar increase is seen in the ^{10}Be concentration from MFM about a hundred
133 years later.

134

135 3.2 Time-scales synchronization

136 The Greenland ice core time-scale is characterized by an accumulating layer counting uncertainty back in time
137 (Rasmussen et al., 2006) as are chronologies based on sediment varve counting such as MFM. In comparison tree
138 ring chronologies, underlying the ^{14}C calibration record, are considered accurate with virtually no dating
139 uncertainty for the Holocene period (Reimer et al., 2013). Considering the different time-scale uncertainties, it is
140 challenging to compare the timing of short-lived climate oscillations such as the PBO/11.4 ka event. Here we use
141 the global signature common to all cosmogenic radionuclide records as a synchronization tool (Muscheler et al.,
142 2008; 2014). More specifically, we use the large fluctuations in both the MFM and GRIP ^{10}Be data to synchronize
143 these records onto the chronologically more accurate and precise IntCal13 time-scale (Czymzik et al., 2018). It
144 was previously shown that GICC05 increasingly overestimates age during the Holocene, compared to IntCal13
145 (Muscheler et al., 2014) and this time-scale difference is estimated to increase to 67 (\pm 6) years at 11,000 years
146 BP (Adolphi and Muscheler, 2016). We use the same Bayesian wiggle-matching approach as in Adolphi and
147 Muscheler (2016), but here for the period 11,000-11,800 years BP to synchronize both the MFM sediment and
148 Greenland ice core records onto IntCal13.

149 Figure 2 shows both the ice-core and sediment-core ^{10}Be data once synchronized onto the IntCal13 time-
150 scale using the ^{14}C production rate from Muscheler et al. (2014), with the corresponding probability density
151 functions displayed on the right-hand panel. We find that the MFM ^{10}Be data fit best with ^{14}C by adding 20 years



152 to MFM2012 (+6/-19 years uncertainty with a 95.4% confidence interval), whereas the GRIP ^{10}Be data fit best
153 with ^{14}C by shifting GICC05 78 years towards present (+32/-8 years uncertainty with a 95.4% likelihood interval).
154 When comparing GICC05 directly to MFM2012, we find that the best fit occurs by shifting GICC05 72 years
155 towards MFM2012 (+4/-8 years with a 95.4% likelihood interval). There is thus a difference of 26 years (72 +4/-
156 8 years vs. 98 +33/-21 years) when comparing GICC05 and MFM2012 directly, rather than synchronizing them
157 to IntCal13 first which illustrates the uncertainties inherent to this exercise. In the following, we will compare
158 GICC05 and MFM2012 when synchronized to IntCal13 as it is the more robust time-scale and thus consider the
159 combined chronology offset of 98 (+33/-21) years. Another uncertainty from these estimates arises from the
160 influence of climate on the cosmogenic signal of all radionuclides (Adolphi et al., 2014; Muscheler et al., 2008;
161 Pedro et al., 2012). For instance, ^{14}C oxidizes to form $^{14}\text{CO}_2$ and enters the carbon cycle while ^{10}Be readily attaches
162 to aerosols and is thus influenced by precipitation. Even though ^{10}Be deposition is not expected to have strong
163 environmental influences at MFM (Czymzik et al., 2016), this was taken into account within the 20% uncertainty
164 since these effects are difficult to quantify objectively.
165

166 3.3 Anomalies in paleoclimate proxies between 11,450-11,000 years BP

167 If we correct the GICC05 and MFM2012 timescales for their respective offsets to IntCal13, we can compare Early
168 Holocene climate in Greenland to data from MFM with a high chronological precision. Figure 3 displays a
169 selection of climate proxies from both Greenland ice cores and the varved MFM record on the IntCal13 time-scale,
170 as per Fig. 2. In addition, both ^{14}C atmospheric production rate and GRIP ^{10}Be concentrations are shown as a
171 general indicator of changes in solar activity (Fig. 3a). The stack of $\delta^{18}\text{O}$ anomalies from four Greenland ice cores
172 (DYE-3, GRIP, NGRIP, and Renland - Fig. 3b) can be related to surface air temperature around Greenland
173 (Rasmussen et al., 2007; Vinther et al., 2009) and shows one negative fluctuation between 11,400-11,250 years
174 BP. Following this oscillation, the Greenland $\delta^{18}\text{O}$ anomaly record remains largely constant and positive. In
175 addition, we also use the accumulation rate anomaly stack (Fig. 3c) from the DYE-3, GRIP, and NGRIP ice cores
176 (Rasmussen et al., 2007) to illustrate changes in snow accumulation rates over Greenland. Here again, a negative
177 fluctuation is observed between 11,400-11,250 years BP. Then, we make use of the MFM δD records of n-alkanes
178 (Fig. 3d) that has been interpreted as a proxy for precipitation δD (Rach et al., 2014) which, similarly to $\delta^{18}\text{O}$ in
179 Greenland, can thus be regarded as indicative of distance from, and temperature/humidity at the moisture source
180 (Dansgaard, 1964) as well as fractionation related to air temperature. As opposed to the Greenland stack, the δD
181 data show no fluctuations between 11,400-11,250 years BP with $\delta\text{D}_{\text{aq}}$ remaining constant and $\delta\text{D}_{\text{terr}}$ showing an
182 increasing trend. Then at 11,250 years BP, both δD series depict a 20% drop that persists until 11,100 years BP.
183 To test the spatial scale to which the δD record from MFM can be representative of, we have investigated the
184 spatial relationship between surface air temperature (SAT) in the NOAA-CIRES 20th climate reanalysis V2c
185 (20CR; Compo et al., 2011) and δD in precipitation from the Trier meteorological station (about 50 km SW of
186 MFM). It can be seen from Fig. 4 that there is a significant relationship ($p < 0.1$) between annual precipitation δD
187 from the Trier station (IAEA/WMO, 2006) and annual SAT over most of western Europe. In addition, Fig. 4 also
188 points to a relationship between annual SATs over Greenland-Iceland and annual $\delta^{18}\text{O}$ at Summit (Steig et al.,
189 1994; White et al., 2009). Finally, we also show varve thickness changes at MFM that were primarily controlled
190 by runoff from the catchment. After a period of low varve thickness, a sharp increase occurred 11,250 years BP



191 followed by a gradual decrease and a second but very small increase around 11,080 years BP. Titanium centered-
192 log ratio data (Ti_{clr}), determined by micro X-ray fluorescence (μ -XRF) from the same MFM sediment composite
193 profile (Martin-Puertas et al., 2017), confirm the interpretation that the variance in varve thickness at the time was
194 mostly controlled by detrital supply to the lake (Fig. 3e). It is important to mention that on a longer time
195 perspective, the changes described above in the sediments of MFM (Martin-Puertas et al., 2017; Rach et al., 2012)
196 do not exceed other fluctuations in varve thickness and Ti_{clr} .
197

198 4 Discussion

199 4.1 Timing and interpretation of anomalies between 11,450-11,000 years BP

200 In Greenland, a cold and dry climate episode occurred around 11,400-11,250 years BP known as the 11.4 ka event
201 (Rasmussen et al., 2007). This is evidenced by a significant drop in the signal of the Greenland ice core $\delta^{18}O$ stack
202 as well as in the accumulation stack (Fig. 3b-c). By shifting GICC05 78 years towards present, this means that the
203 central part of the 11.4 ka event (lowest value in $\delta^{18}O$) is dated to about 11,372-11,272 (+32/-8) years BP which
204 is consistent with GICC05 within the combined uncertainty of our synchronization and the maximum counting
205 error in GICC05. When looking at the temperature proxy and varve thickness from MFM (Fig. 3d-e), we do not
206 find any event that is coeval with the 11.4 ka event in Greenland. Interestingly though, Ti_{clr} data (Fig. 3e) gradually
207 decreased from ca. 11,490 years BP only to be interrupted by a small increase around 11,300 years BP. The low
208 Ti_{clr} data suggest less runoff probably related to drier conditions. Therefore, a possible link to the dry “Rammelbeek
209 Phase” described from the Borchert peat sequence in the Netherlands (van der Plicht et al., 2004; Bos et al., 2007)
210 may be tentatively put forward although chronological uncertainties hinder proving this. We can now also
211 confidently deduce that the termination of the $\delta^{18}O$ and accumulation anomalies in Greenland (the 11.4 ka event)
212 is synchronous with a large decrease in solar activity (Fig. 3a-c). More specifically, high levels of solar activity
213 prevailed throughout the occurrence of the 11.4 ka event in Greenland. Then as solar activity started to decrease
214 (circa 11,250 years BP) into a grand solar minimum that lasted for about 250 years, climate in Greenland switched
215 back to warmer and wetter conditions with higher $\delta^{18}O$ values and accumulation rate. This is in accordance with
216 the suggestion of an abrupt warming ($4^\circ \pm 1.5^\circ$) in Greenland following the event, based on $\delta^{15}N$ in the GIPS2 ice
217 core (Kobashi et al., 2008). The rapid transition towards positive accumulation anomalies occurred over a few
218 decades only.

219 While climate over Greenland following the 11.4 ka event returned rapidly to warmer and wetter
220 conditions, all proxies from MFM sediments (Fig. 3d-e) show fluctuations around 11,250 years BP (henceforth
221 MFM oscillation). In particular, aquatic δD data from small-chain alkanes (Rach et al., 2014) show a clear
222 oscillation with a 20% drop around 11,250 years BP (Fig. 3d) while terrestrial δD data show a decrease reaching
223 levels seen about 11,500 years BP. This deuterium depletion in the alkanes most likely mirrors a depletion of
224 deuterium in precipitation which can be explained, in part, by lower air temperatures over western Europe in view
225 of Fig. 4. Simultaneously, varve thickness and Ti_{clr} show a rapid increase at 11,250 years BP (Fig. 3e) denoting a
226 likely increasing detrital contribution to this varve thickening. When considered into a longer time perspective
227 (Martin-Puertas et al., 2017), this varve increase reaches the level of other fluctuations that are unrelated to known
228 Early Holocene oscillations in North-Atlantic climate. Nevertheless, this shift at 11,250 year BP does correspond



229 to a change in the composition of the sediments as Martin-Puertas et al. (2017) defined a compositional boundary
230 of MFM varves at 11,230 years BP (11,250 years BP on the IntCal13 time-scale), based on μ -XRF scanning
231 analyzed with Ward's clustering methods. By synchronizing MFM2012 onto IntCal13 (Fig. 2), we find that this
232 compositional boundary is also coeval with the onset of the grand solar minimum (Fig. 3) although the cause of
233 this change is difficult to assess. In fact, Ti_{clr} as well as $\ln(Si/Ti)$ and $\ln(Ca/Ti)$, generally regarded by Martin-
234 Puertas et al. (2017) as indicating relative changes of biogenic silica concentrations and authigenic calcite
235 precipitation, are significantly correlated to the new ^{10}Be concentration measurements, but also to the GRIP ^{10}Be
236 data and to ^{14}C atmospheric production rate (Fig. 5 and Sup. Fig. 1). Because GRIP ^{10}Be concentrations and ^{14}C
237 atmospheric production rate are unaffected by environmental changes at MFM, we suggest that the catchment area
238 of MFM was likely influenced by the substantial changes in solar activity that characterized this period rather than
239 ^{10}Be concentration at MFM being affected by this sediment compositional change. In support to this assumption,
240 Czymzik et al. (2016) also reported negligible climate influences on ^{10}Be deposition at MFM, even across distinct
241 climatological boundaries. It can also be seen that the second and smaller increase in varve thickness and Ti_{clr} is
242 coeval with a second dip in solar activity shortly after 11,100 years BP (Fig. 3a and 3e). Finally, it is worthwhile
243 to note that the percentage values of *Pinus* pollen, biogenic silica, as well as pollen concentrations in MFM all
244 decreased at 11,230-11,250 years BP while percentage values of *Betula* increased (Brauer et al., 1999). Although
245 not interpreted by the authors, these changes echo to the findings of Björck et al. (1997) who defined the PBO in
246 terrestrial records of Sweden with a similar decrease of pollen concentrations and more notably of *Pinus* pollen
247 percentages, interpreted as a set-back of tree vegetation in Southern Sweden. It should be stressed here that we
248 cannot directly compare the palynology of MFM to these Swedish lakes because of the challenging interpretation
249 of the former record as well as the chronology uncertainties and vicinity to the retreating Fennoscandian Ice Sheet
250 of the latter records.

251 In summary, the radionuclide-based synchronization of the GICC05 and MFM2012 time-scales indicate
252 a combined timing offset of up to 98 (+33/-21) years during the earliest part of the Holocene. Correcting for this
253 offset, we observe that cold oscillations at both locations and inferred from water isotopes did not occur
254 simultaneously between 11,450 and 11,000 years BP. We further note that this pattern appears to be coupled with
255 large changes in solar activity, which leads us to suggest a causal link. More specifically, the cold and dry climate
256 oscillation in Greenland (the 11.4 ka event) occurred under a period of high solar activity between c. 11,370-
257 11,270 years BP, but did not leave a discernable imprint in either varve thickness or biomarker δD from MFM.
258 Subsequently, solar activity dropped to a grand minimum that lasted for as long as 250 years. This change was
259 coeval with the termination of the 11.4 ka event (Greenland) and the onset of the MFM oscillation with colder
260 conditions inferred from δD data (Figs. 3d and 4). The ostensible link with solar activity which we infer in view
261 of Fig. 3 resembles to what has been described substantially in the recent literature and is discussed in the following
262 section.

263

264 4. 2 Solar forcing during 11,450-11,000 years BP

265 Our suggestion of a causal sun-climate link during the earliest part of the Holocene can be further supported by
266 the spatial patterns of the 11.4 ka event in Greenland followed by a cold period at MFM starting at 11,250 years
267 BP (MFM oscillation). Based on our synchronization of the different paleoclimate records, we find an



268 asynchronous relationship between Greenlandic and European climate, characterized by cold and dry conditions
269 over Greenland, but with no evidence of it at MFM, under high solar activity and a warm and wetter Greenlandic
270 climate as well as a colder conditions at MFM for low solar activity (Fig. 3).

271 This pattern is consistent with a number of, but not all, climate modeling studies that find a top-down
272 influence of solar activity on North Atlantic/European atmospheric circulation patterns. This forcing mechanism
273 involves the increase in UV radiation during solar maxima years (Haigh et al., 2010; Lockwood et al., 2010) which
274 enhances the production of stratospheric ozone and leads to stratospheric heating through increased absorption of
275 long wave radiation (Haigh et al., 2010) especially at the equator. This increases the stratospheric temperature
276 gradient between the equator and poles (Simpson et al., 2009) leading to an acceleration of the polar night jet
277 (Kodera et al., 2002), which eventually propagates down to the troposphere via wave refraction (Matthes et al.,
278 2006; Ineson et al., 2011). In turn, this leads to patterns in surface pressure and temperature which mimic those of
279 the positive phase of the North Atlantic Oscillation in winter (Woollings et al., 2010; Ineson et al., 2011). The
280 opposite mode applies during periods of solar minima. It should however be stressed that there is no consistent
281 correlation between the NAO and solar forcing for the past centuries (Gray et al., 2013; Ortega et al., 2015)
282 although a solar influence on the region is not necessarily related to the NAO (Moffa-Sánchez et al., 2014; Sjolte
283 et al., 2018). Even though the spatial pattern we observe agrees well with a top-down solar forcing, other
284 mechanisms cannot be excluded to lie behind the different North-Atlantic response patterns. Overall, it has to be
285 kept in mind that different time periods with different climate boundaries could lead to shifting atmospheric
286 patterns.

287 In the following we explore the solar hypothesis further by investigating a modern analogue with climate
288 reanalysis data. Figure 6a shows the surface air temperature (SAT) anomalies in the North Atlantic region for
289 periods of solar maxima compared to periods of solar minima in 20CR (mean $\pm 1\sigma$ of the sunspot group numbers
290 from Svalgaard and Schatten (2016) between 1946-2011, see Sup. Fig. 2). It can be seen from the SAT anomalies
291 that a distinct antiphase pattern between Greenland and Europe is coincident with highs and lows in solar activity.
292 That is, Greenland experiences lower SATs during winters of solar maxima compared to winters of solar minima
293 whereas lower SATs are observed across Europe for winters of solar minima compared to winters of solar maxima.
294 This highlights the correspondence between the solar influence on North-Atlantic climate which has been proposed
295 to act during the 20th century and the synchronized climate proxy records during the Early Holocene, in terms of
296 spatial distribution of SAT anomalies. Furthermore, this correspondence can also be qualitatively described by
297 comparing the mean annual temperature anomalies at both Summit (central Greenland) and MFM (Fig. 6c-d)
298 throughout an average of all 11-year solar cycles of the 20th century (Fig. 6b). Decadal temperature changes in
299 20CR at both Summit (blue curve in Fig. 6c) and MFM (red curve in Fig. 6d) agree qualitatively well with
300 centennial $\delta^{18}\text{O}$ and δD changes observed in Greenland ice cores and in MFM sediments and during the period
301 ranging from 11,450 to 11,000 years BP (black curves in Fig. 6c-d, note the different time-axes). Of specific interest
302 here is the average transition from high to low solar activity that is coincident with an annual temperature rise/drop
303 of ca. 1K at Summit/MFM. Assuming changes in water isotopes to be, in part, indicative of regional temperature
304 changes (Dansgaard, 1964; Masson-Delmotte et al., 2005; Rach et al., 2014; Fig. 4), this decadal pattern between
305 Summit and MFM in climate reanalysis data mimics the centennial-scale climate changes that prevailed in
306 Greenland and Europe throughout 11,450-11,000 years BP. Water isotopes are often dominated by a particular



307 seasonal signal. It is therefore of interest to note that the spatial patterns observed in climate reanalysis is also
308 present during the summer, although to a lesser degree (Sup. Fig. 3).

309 It should be noted that the efficiency of the top-down mechanism remains largely unexplored for
310 centennial time-scales. For instance, previous studies have proposed a top-down solar influence on atmospheric
311 circulation on similar time-scales for both Greenland (Adolphi et al., 2014) and MFM (Martin-Puertas et al.,
312 2012b) leading to a similar spatial pattern in reanalysis data. The modeling results in these studies do however
313 only investigate the effect of decadal (11-years) changes in solar activity. In contrast, it was also shown more
314 recently that the centennial response of North-Atlantic atmospheric circulation to solar forcing is correlated to the
315 second mode of atmospheric circulation, the Eastern Atlantic Pattern, rather than to the first mode, the NAO (Sjolte
316 et al., 2018). The latter study consequently does not find a similar pattern in SAT anomalies between Greenland
317 and western Europe.

318 For the same reasons, another uncertainty arises from the relevance of using 20th century climate
319 reanalysis as an analogy of Early Holocene conditions. In particular, the Laurentide ice sheet (LIS) is known to
320 have played an important role in the position of the North Atlantic eddy-driven jet by accelerating and displacing
321 it southward (Merz et al., 2015). However, it is also known that the LIS waned to the point of separation with the
322 Cordilleran at about 14,000 years BP (Dyke, 2004). According to a study based on a transient climate simulation
323 from the LGM (Löfverström and Lora, 2017), this separation led to a shift in the dominant topographic stationary
324 wave source in North America. This, in turn, induced a transition from a strong and subtropical jet stream to a
325 weaker and more meridionally tilted jet stream and storm track, as observed for present conditions. This suggests
326 that similar atmospheric processes could have been at play during the earliest part of the Holocene, relative to
327 today, in spite of different boundary conditions. Furthermore, the results from Fig. 6 arise from an 11-year solar
328 cycle forcing which is considerably weaker and less persistent than the potential solar forcing that the 11,400 years
329 BP solar maximum to 11,200 years BP grand solar minimum could have provoked, leading to possibly different
330 reactions due to feedback processes. In fact, both the ¹⁴C data and GRIP ¹⁰Be data shown in Fig. 2 depict one of
331 the most prominent increases of the Holocene record (Vonmoos et al., 2006), in terms of both amplitude and
332 duration of the grand solar minimum. In comparison, its duration represents twice the length of the longest grand
333 minimum known from sunspot observations (Svalgaard and Schatten, 2016) and called the Maunder minimum.
334

335 4.3 Solar-ocean coupling

336 The PBO has also been associated with an increase in freshwater supply hampering the Atlantic meridional
337 overturning circulation (AMOC), possibly from the Baltic Ice Lake drainage and the rapidly waning
338 Fennoscandian ice sheet (Björck et al., 1996; Hald and Hagen, 1998). It was next proposed by Fisher et al. (2002)
339 that an outburst of Lake Agassiz could represent the trigger of the PBO through an increased thickness and extent
340 of Arctic Ocean sea-ice pack. This would have resulted in an increased albedo as well as a slowdown of North
341 Atlantic Deep Waters (NADW) formation due to increased freshwater delivery to the North Atlantic. However,
342 the timing of the outburst event of which they attribute the PBO to (11,335 cal yr BP) has rather large uncertainties
343 (± 130 to 230 years) due to the $\Delta^{14}\text{C}$ age plateau at this period. More recently, it was suggested that even small
344 changes in the prevalence of the AMOC can influence atmospheric circulation with couplings to the NAO with an
345 intensification of the former resulting in a negative index of the latter (Frankignoul et al., 2013).



346 To further investigate the potential spatial distribution of SAT anomalies due to a slowdown of the
347 AMOC, we again investigate 20CR for winters with a negative reconstructed AMOC index (Duchez et al., 2014)
348 compared to winters with a positive reconstructed AMOC index for the period 1961-2005 (Fig. 7a). Interestingly,
349 similar SAT anomalies subside as those for solar forcing. That is, an amplified meridional temperature gradient
350 with a colder Greenland and warmer western Europe are favoured in winters where the AMOC is weaker, relative
351 to winters where it is stronger. Although it is difficult to obtain direct evidence of an AMOC slowdown during the
352 Early Holocene, it is conceivable that the waning Fennoscandian ice sheet would have released routinely enough
353 freshwater to weaken and condition the AMOC for the onset of the 11.4 ka event in Greenland. This result could
354 also be explained by the influence of the NAO on the AMOC index, as it is difficult to detangle these tightly
355 coupled processes (McCarthy et al., 2015). In this case, the persistent high levels of solar activity, which also can
356 favor such temperature and pressure patterns, could represent a potential trigger for these climate oscillations.
357 Figure 7b depicts the large temperature differences for winters where both high solar activity and a weak AMOC
358 prevailed during the period 1961-2005, with up to a -4K anomaly in western Greenland. This however needs to be
359 treated with caution due to the relatively short period of observation that results in very few years where such solar
360 activity and AMOC conditions existed in parallel (Sup. Fig. 4).

361 In addition, a coupling between solar and freshwater forcing could also explain the lack of significant
362 climate responses to subsequent grand solar minima which were also large in amplitude but did not yield an
363 unequivocal impact on North Atlantic climate. It is indeed notable that the following changes in solar activity
364 occurred while the influence of freshwater release by the FIS was diminishing, and therefore the North Atlantic
365 was not conditioned as it was during the PBO. For instance, a similar but weaker event was found in the $\delta^{18}\text{O}$
366 signal of the GRIP ice core around 10,300 cal. years BP, coinciding with a low in $\Delta^{14}\text{C}$ (high solar activity) and a
367 cooling in the Faroe Islands (Björck et al., 2001). Whereas, the subsequent grand solar minimum which occurred
368 around 9,500 years BP (Vonmoos et al., 2006), at a time during which the FIS had completely vanished (Stroeven
369 et al., 2016), did not coincide with any evident climate oscillation in Greenland.
370

371 5 Conclusions

372 A comparison of new ^{10}Be concentration measurements from the varved Meerfelder Maar sediments covering the
373 period 11,310-11,000 years BP to the ^{10}Be data from the GRIP ice core in central Greenland showed a combined
374 offset of up to 98 (+33/-21) years between the MFM2012 and GICC05 chronologies. Correcting for this offset
375 allowed us to determine that the 11.4 ka event in Greenland has no coeval counterparts in Meerfelder Maar and
376 that it coincides with high solar activity. The time-scales synchronization also showed that an environmental shift
377 at MFM starting at 11,250 years BP is coincident with a transition from high solar activity to a particularly long-
378 lasting grand solar minimum as well as with the termination of the 11.4 ka event in Greenland. The termination
379 and onset of these cold oscillations in Greenland and then Meerfelder Maar are thus synchronous with large
380 changes in solar activity which is a pattern reproduced by a number of modeling studies. Finally, we also postulate
381 that a slowdown of the AMOC due to freshwater delivery from, for instance, the Fennoscandian Ice Sheet could
382 have served as a potential amplifier to this signal. The extent of the role that solar activity changes may have
383 played on the climate of Greenland and Europe during the earliest part of the Holocene is unclear. This is due to



384 the different boundary conditions which prevailed at the time compared to today but also to the proxy-evidence
385 from MFM which is difficult to interpret. The main results from this study do however exemplify the usefulness
386 of cosmogenic radionuclides to synchronize different paleo-records in an effort to investigate the timing and spatial
387 distribution of past climate fluctuations with a high chronological precision.

388

389 **Author contribution:** FM performed the analysis in correspondence with RM, carried out the sampling with MC
390 and CMP, and did the chemical preparation of the Meerfelder Maar ^{10}Be samples with help of AA while GP
391 performed the measurements. FM wrote the manuscript. RM, MC, and FM initiated the project. FA provided the
392 Bayesian synchronization and participated in the interpretation of climate reanalysis with JS. SB, AB, MC, and
393 CMP assisted with the interpretation of the proxy data. All authors were involved in editing the manuscript.

394

395 **Data availability:** The new ^{10}Be data connected to this study have been submitted to the PANGAEA open access
396 data library.

397 **Competing interests:** The authors declare that they have no conflict of interest.

398

399 Acknowledgements

400 This work was supported by the Royal Physiographic Society of Lund (grant to FM) and the Swedish Research
401 Council (grant DNR2013-8421 to RM). MC was funded by a grant from the German Research Foundation (DFG
402 grant CZ 227/4-1) and the BaltRap network of the Leibniz Association SAW-2017-IOW2). FA was supported by
403 the Swedish research council (grant DNR2016-00218). ssAA thanks the UAEU for support through the UPAR
404 funding. The authors would like to thank Inger Pålsson for her help with the chemical preparation of the sediment
405 ^{10}Be samples for AMS measurements.

406 References

- 407 Adolphi, F., and Muscheler, R.: Synchronizing the Greenland ice core and radiocarbon time-scales over the
408 Holocene – Bayesian wiggle-matching of cosmogenic radionuclide records, *Clim. Past*, 12(1), 15–30,
409 doi:10.5194/cp-12-15-2016, 2016.
- 410 Adolphi, F., Muscheler, R., Svensson, A., Aldahan, A., Possnert, G., Beer, J., Sjolte, J., Björck, S., Matthes, K.
411 and Thiéblemont, R.: Persistent link between solar activity and Greenland climate during the Last Glacial
412 Maximum, *Nat. Geosci.*, 7(9), 662–666, doi:10.1038/ngeo2225, 2014.
- 413 Berggren, A.-M., Aldahan, A., Possnert, G., Haltia-Hovi, E. and Saarinen, T.: ^{10}Be and solar activity cycles in
414 varved lake sediments, AD 1900–2006, *J. Paleolimnol.*, 44(2), 559–569, doi:10.1007/s10933-010-9437-1,
415 2010.
- 416 Bos, J. A. A., van Geel, B., van der Plicht, J. and Bohncke, S. J. P.: Preboreal climate oscillations in Europe:
417 Wiggle-match dating and synthesis of Dutch high-resolution multi-proxy records, *Quat. Sci. Rev.*, 26(15–
418 16), 1927–1950, doi:10.1016/j.quascirev.2006.09.012, 2007.



- 419 Björck, S., Kromer, B., Johnsen, S., Bennike, O., Hammarlund, D., Lemdahl, G., Possnert, G., Rasmussen, T. L.,
420 Wohlfarth, B., Hammer, C. U. and Spurk, M.: Synchronized Terrestrial-Atmospheric Deglacial Records
421 Around the North Atlantic, *Science*, 274(5290), 1155–60, doi:10.1126/SCIENCE.274.5290.1155, 1996.
- 422 Björck, S., Rundgren, M., Ingólfsson, Ó. and Funder, S.: The Preboreal oscillation around the Nordic Seas:
423 terrestrial and lacustrine responses, *J. Quat. Sci.*, 12(6), 455–465, doi:10.1002/(SICI)1099-
424 1417(199711/12)12:6<455::AID-JQS316>3.0.CO;2-S, 1997.
- 425 Björck, S., Muscheler, R., Kromer, B., Andresen, C. S., Heinemeier, J., Johnsen, S. J., Conley, D., Koç, N., Spurk,
426 M. and Veski, S.: High-resolution analyses of an early Holocene climate event may imply decreased solar
427 forcing as an important climate trigger, *Geology*, 29(12), 1107, doi:10.1130/0091-
428 7613(2001)029<1107:HRAOAE>2.0.CO;2, 2001.
- 429 Brauer, A., Endres, C., Günter, C., Litt, T., Stebich, M. and Negendank, J. F. W.: High resolution sediment and
430 vegetation responses to Younger Dryas climate change in varved lake sediments from Meerfelder Maar,
431 Germany, *Quat. Sci. Rev.*, 18(3), 321–329, doi:10.1016/S0277-3791(98)00084-5, 1999.
- 432 Brauer, A., Endres, C., Zolitschka, B. and Negendank, J. F.: AMS radiocarbon and varve chronology from the
433 annually laminated sediment record of Lake Meerfelder Maar, Germany. *Radiocarbon*, 42(3), 355-368,
434 2000.
- 435 Compo, G. P., Whitaker, J. S., Sardeshmukh, P. D., Matsui, N., Allan, R. J., Yin, X., Gleason, B. E., Vose, R. S.,
436 Rutledge, G., Bessemoulin, P., Brönnimann, S., Brunet, M., Crouthamel, R. I., Grant, A. N., Groisman, P.
437 Y., Jones, P. D., Kruk, M. C., Kruger, A. C., Marshall, G. J., Mauerer, M., Mok, H. Y., Nordli, Ø., Ross, T.
438 F., Trigo, R. M., Wang, X. L., Woodruff, S. D. and Worley, S. J.: The Twentieth Century Reanalysis Project,
439 *Q. J. R. Meteorol. Soc.*, 137(654), 1–28, doi:10.1002/qj.776, 2011.
- 440 Czymzik, M., Adolphi, F., Muscheler, R., Mekhaldi, F., Martin-Puertas, C., Aldahan, A., Oran Possnert, G. € and
441 Brauer, A.: A varved lake sediment record of the ¹⁰Be solar activity proxy for the Lateglacial-Holocene
442 transition, *Quat. Sci. Rev.*, 153, 31–39, doi:10.1016/j.quascirev.2016.10.007, 2016.
- 443 Czymzik, M., Muscheler, R., Adolphi, F., Mekhaldi, F., Dräger, N., Ott, F., Slowinski, M., Blaszkiewicz, M.,
444 Aldahan, A., Possnert, G. and Brauer, A.: Synchronizing ¹⁰Be in two varved lake sediment records to
445 IntCal13 ¹⁴C during three grand solar minima, *Clim. Past*, 14(5), doi:10.5194/cp-14-687-2018, 2018.
- 446 Dansgaard, W.: Stable isotopes in precipitation, *Tellus*, 16(4), 436–468, doi:10.3402/tellusa.v16i4.8993, 1964.
- 447 Duche, A., Hirschi, J. J.-M., Cunningham, S. A., Blaker, A. T., Bryden, H. L., De Cuevas, B., Atkinson, C. P.,
448 Mccarthy, G. D., Frajka-Williams, E., Rayner, D., Smeed, D. and Mizielinski, M. S.: A new index for the
449 Atlantic Meridional Overturning Circulation at 26°N., *J. of Clim.*, 27(17), 6439-6455, doi:10.1175/JCLI-D-
450 13-00052.1, 2014.
- 451 Dyke, A. S.: An outline of North American deglaciation with emphasis on central and northern Canada, *Dev. in*
452 *Quat. Sci.*, 2, 373-424, doi.org/10.1016/S1571-0866(04)80209-4, 2004.
- 453 Finkel, R. C. and Nishiizumi, K.: Beryllium 10 concentrations in the Greenland Ice Sheet Project 2 ice core from
454 3–40 ka, *J. Geophys. Res. Ocean.*, 102(C12), 26699–26706, doi:10.1029/97JC01282, 1997.
- 455 Fisher, T. G., Smith, D. G. and Andrews, J. T.: Preboreal oscillation caused by a glacial Lake Agassiz flood, *Quat.*
456 *Sci. Rev.*, 21(8–9), 873–878, doi:10.1016/S0277-3791(01)00148-2, 2002.
- 457 Frankignoul, C., Gastineau, G. and Kwon, Y. O.: The influence of the AMOC variability on the atmosphere in
458 CCSM3, *J. of Clim.*, 26(24), 9774-9790, doi.org/10.1175/JCLI-D-12-00862.1, 2013.



- 459 Gray, L. J., Scaife, A. A., Mitchell, D. M., Osprey, S., Ineson, S., Hardiman, S., Butchart, N., Knight, J., Sutton,
460 R. and Kodera, K.: A lagged response to the 11 year solar cycle in observed winter Atlantic/European
461 weather patterns, *J. Geophys. Res. Atmos.*, 118(24), 13,405–13,420, doi:10.1002/2013JD020062, 2013.
- 462 Haigh, J. D., Winning, A. R., Toumi, R. and Harder, J. W.: An influence of solar spectral variations on radiative
463 forcing of climate, *Nature*, 467(7316), 696–699, doi:10.1038/nature09426, 2010.
- 464 Hald, M. and Hagen, S.: Early Preboreal cooling in the Nordic seas region triggered by meltwater, *Geology*,
465 doi:10.1130/0091-7613(1998)026<0615:EPCITN>2.3.CO;2, 1998.
- 466 Ineson, S., Scaife, A. A., Knight, J. R., Manners, J. C., Dunstone, N. J., Gray, L. J. and Haigh, J. D.: Solar forcing
467 of winter climate variability in the Northern Hemisphere, *Nat. Geosci.*, 4(11), 753–757,
468 doi:10.1038/ngeo1282, 2011.
- 469 Kobashi, T., Severinghaus, J. P. and Barnola, J.-M.: 4 ± 1.5 °C abrupt warming 11,270 yr ago identified from
470 trapped air in Greenland ice, *Earth Planet. Sci. Lett.*, 268(3–4), 397–407, doi:10.1016/j.epsl.2008.01.032,
471 2008.
- 472 Kodera, K.: Solar cycle modulation of the North Atlantic Oscillation: Implication in the spatial structure of the
473 NAO, *Geophys. Res. Lett.*, 29(8), 59-1-59–4, doi:10.1029/2001GL014557, 2002.
- 474 Lane, C. S., Brauer, A., Martín-Puertas, C., Blockley, S. P. E., Smith, V. C. and Tomlinson, E. L.: The Late
475 Quaternary tephrostratigraphy of annually laminated sediments from Meerfelder Maar, Germany, *Quat. Sci.*
476 *Rev.*, 122, 192–206, doi:10.1016/j.quascirev.2015.05.025, 2015.
- 477 Lockwood, M., Bell, C., Woollings, T., Harrison, R. G., Gray, L. J. and Haigh, J. D.: Top-down solar modulation
478 of climate: evidence for centennial-scale change, *Environ. Res. Lett.*, 5(3), 34008, doi:10.1088/1748-
479 9326/5/3/034008, 2010.
- 480 Löffverström, M. and Lora, J. M.: Abrupt regime shifts in the North Atlantic atmospheric circulation over the last
481 deglaciation, *Geophys. Res. Lett.*, 44(15), 8047–8055, doi:10.1002/2017GL074274, 2017.
- 482 Magny, M., Vanni re, B., de Beaulieu, J.-L., B geot, C., Heiri, O., Millet, L., Peyron, O. and Walter-Simonnet,
483 A.-V.: Early-Holocene climatic oscillations recorded by lake-level fluctuations in west-central Europe and
484 in central Italy, *Quat. Sci. Rev.*, 26(15–16), 1951–1964, doi:10.1016/j.quascirev.2006.04.013, 2007.
- 485 Martin-Puertas, C., Brauer, A., Dulski, P. and Brademann, B.: Testing climate–proxy stationarity throughout the
486 Holocene: an example from the varved sediments of Lake Meerfelder Maar (Germany), *Quat. Sci. Rev.*, 58,
487 56–65, doi:10.1016/J.QUASCIREV.2012.10.023, 2012a.
- 488 Martin-Puertas, C., Matthes, K., Brauer, A., Muscheler, R., Hansen, F., Petrick, C., Aldahan, A., Possnert, G. and
489 van Geel, B.: Regional atmospheric circulation shifts induced by a grand solar minimum, *Nat. Geosci.*, 5(6),
490 397–401, doi:10.1038/ngeo1460, 2012b.
- 491 Martin-Puertas, C., Tjallingii, R., Bloemsm a, M. and Brauer, A.: Varved sediment responses to early Holocene
492 climate and environmental changes in Lake Meerfelder Maar (Germany) obtained from multivariate
493 analyses of micro X-ray fluorescence core scanning data, *J. Quat. Sci.*, 32(3), 427–436,
494 doi:10.1002/jqs.2935, 2017.
- 495 Masson-Delmotte, V., Landais, A., Stievenard, M., Cattani, O., Falourd, S., Jouzel, J., Johnsen, S. J., Dahl-Jensen,
496 D., Sveinbjornsdottir, A., White, J. W. C., Popp, T. and Fischer, H.: Holocene climatic changes in
497 Greenland: Different deuterium excess signals at Greenland Ice Core Project (GRIP) and NorthGRIP, *J.*
498 *Geophys. Res. Atmos.*, 110(D14), n/a-n/a, doi:10.1029/2004JD005575, 2005.



- 499 Matthes, K., Kuroda, Y., Kodera, K. and Langematz, U.: Transfer of the solar signal from the stratosphere to the
500 troposphere: Northern winter, *J. Geophys. Res.*, 111(D6), D06108, doi:10.1029/2005JD006283, 2006.
- 501 McCarthy, G. D., Haigh, I. D., Hirschi, J. J. M., Grist, J. P., and Smeed, D. A.: Ocean impact on decadal Atlantic
502 climate variability revealed by sea-level observations, *Nature*, 521(7553), 508, doi:10.1038/nature14491,
503 2015.
- 504 Merz, N., Raible, C. C. and Woollings, T.: North Atlantic Eddy-Driven Jet in Interglacial and Glacial Winter
505 Climates, *J. Clim.*, 28(10), 3977–3997, doi:10.1175/JCLI-D-14-00525.1, 2015.
- 506 Moffa-Sánchez, P., Born, A., Hall, I. R., Thornalley, D. J. R. and Barker, S.: Solar forcing of North Atlantic surface
507 temperature and salinity over the past millennium, *Nat. Geosci.*, 7(4), 275–278, doi:10.1038/ngeo2094,
508 2014.
- 509 Muscheler, R., Beer, J., Wagner, G., Laj, C., Kissel, C., Raisbeck, G. M., Yiou, F. and Kubik, P. W.: Changes in
510 the carbon cycle during the last deglaciation as indicated by the comparison of ¹⁰Be and ¹⁴C records, *Earth
511 Planet. Sci. Lett.*, 219(3–4), 325–340, doi:10.1016/S0012-821X(03)00722-2, 2004.
- 512 Muscheler, R., Kromer, B., Björck, S., Svensson, A., Friedrich, M., Kaiser, K. F. and Southon, J.: Tree rings and
513 ice cores reveal ¹⁴C calibration uncertainties during the Younger Dryas, *Nat. Geosci.*, 1(4), 263–267,
514 doi:10.1038/ngeo128, 2008.
- 515 Muscheler, R., Adolphi, F. and Knudsen, M. F.: Assessing the differences between the IntCal and Greenland ice-
516 core time scales for the last 14,000 years via the common cosmogenic radionuclide variations, *Quat. Sci.
517 Rev.*, 106, 81–87, doi:10.1016/J.QUASCIREV.2014.08.017, 2014.
- 518 Ortega, P., Lehner, F., Swingedouw, D., Masson-Delmotte, V., Raible, C. C., Casado, M. and Yiou, P.: A model-
519 tested North Atlantic Oscillation reconstruction for the past millennium, *Nature*, 523(7558), 71–74,
520 doi:10.1038/nature14518, 2015.
- 521 Pedro, J. B., McConnell, J. R., Van Ommen, T. D., Fink, D., Curran, M. A. J., Smith, A. M., Simon, K. J., Moy,
522 A. D. and Das, S. B.: Solar and climate influences on ice core ¹⁰Be records from Antarctica and Greenland
523 during the neutron monitor era, *Aust. Nucl. Sci. Technol. Organ.*, doi:10.1016/j.epsl.2012.08.038, 2012.
- 524 Rach, O., Brauer, a., Wilkes, H. and Sachse, D.: Delayed hydrological response to Greenland cooling at the onset
525 of the Younger Dryas in western Europe, *Nat. Geosci.*, 7(2), 109–112, doi:10.1038/ngeo2053, 2014.
- 526 Rasmussen, S. O., Andersen, K. K., Svensson, A. M., Steffensen, J. P., Vinther, B. M., Clausen, H. B., Siggaard-
527 Andersen, M.-L., Johnsen, S. J., Larsen, L. B., Dahl-Jensen, D., Bigler, M., Röthlisberger, R., Fischer, H.,
528 Goto-Azuma, K., Hansson, M. E. and Ruth, U.: A new Greenland ice core chronology for the last glacial
529 termination, *J. Geophys. Res.*, 111(D6), D06102, doi:10.1029/2005JD006079, 2006.
- 530 Rasmussen, S. O., Vinther, B. M., Clausen, H. B. and Andersen, K. K.: Early Holocene climate oscillations
531 recorded in three Greenland ice cores, *Quat. Sci. Rev.*, 26(15–16), 1907–1914,
532 doi:10.1016/j.quascirev.2007.06.015, 2007.
- 533 Rasmussen, S. O., Bigler, M., Blockley, S. P., Blunier, T., Buchardt, S. L., Clausen, H. B., Cvijanovic, I., Dahl-
534 Jensen, D., Johnsen, S. J., Fischer, H., Gkinis, V., Guillevic, M., Hoek, W. Z., Lowe, J. J., Pedro, J. B., Popp,
535 T., Seierstad, I. K., Steffensen, J. P., Svensson, A. M., Vallenga, P., Vinther, B. M., Walker, M. J. C.,
536 Wheatley, J. J. and Winstrup, M.: A stratigraphic framework for abrupt climatic changes during the Last
537 Glacial period based on three synchronized Greenland ice-core records: refining and extending the



- 538 INTIMATE event stratigraphy, *Quat. Sci. Rev.*, 106, 14–28, doi:10.1016/J.QUASCIREV.2014.09.007,
539 2014.
- 540 Reimer, P. J., Bard, E., Bayliss, A., Beck, J. W., Blackwell, P. G., Ramsey, C. B., Buck, C. E., Cheng, H., Edwards,
541 R. L., Friedrich, M., Grootes, P. M., Guilderson, T. P., Hafliðason, H., Hajdas, I., Hatté, C., Heaton, T. J.,
542 Hoffmann, D. L., Hogg, A. G., Hughen, K. A., Kaiser, K. F., Kromer, B., Manning, S. W., Niu, M., Reimer,
543 R. W., Richards, D. A., Scott, E. M., Southon, J. R., Staff, R. A., Turney, C. S. M. and van der Plicht, J.:
544 IntCal13 and Marine13 Radiocarbon Age Calibration Curves 0–50,000 Years cal BP, *Radiocarbon*, 55(4),
545 1869–1887, doi:10.2458/azu_js_rc.55.16947, 2013.
- 546 Seierstad, I. K., Abbott, P. M., Bigler, M., Blunier, T., Bourne, A. J., Brook, E., Buchardt, S. L., Buizert, C.,
547 Clausen, H. B., Cook, E., Dahl-Jensen, D., Davies, S. M., Guillevic, M., Johnsen, S. J., Pedersen, D. S.,
548 Popp, T. J., Rasmussen, S. O., Severinghaus, J. P., Svensson, A. and Vinther, B. M.: Consistently dated
549 records from the Greenland GRIP, GISP2 and NGRIP ice cores for the past 104 ka reveal regional
550 millennial-scale $\delta^{18}\text{O}$ gradients with possible Heinrich event imprint, *Quat. Sci. Rev.*, 106, 29–46,
551 doi:10.1016/J.QUASCIREV.2014.10.032, 2014.
- 552 Simpson, I. R., Blackburn, M., Haigh, J. D., Simpson, I. R., Blackburn, M. and Haigh, J. D.: The Role of Eddies
553 in Driving the Tropospheric Response to Stratospheric Heating Perturbations, *J. Atmos. Sci.*, 66(5), 1347–
554 1365, doi:10.1175/2008JAS2758.1, 2009.
- 555 Sjolte, J., Sturm, C., Adolphi, F., Vinther, B. M., Werner, M., Lohmann, G. and Muscheler, R.: Solar and volcanic
556 forcing of North Atlantic climate inferred from a process-based reconstruction, *Clim. Past*, 14, 1179–1194,
557 doi:10.5194/cp-14-1179-2018, 2018.
- 558 Southon, J.: A First Step to Reconciling the GRIP and GISP2 Ice-Core Chronologies, 0–14,500 yr B.P., *Quat.*
559 *Res.*, 57(1), 32–37, doi:10.1006/qres.2001.2295, 2002.
- 560 Steig, E.J., Grootes, P.M. and Stuiver, M.: Seasonal Precipitation Timing and Ice Core Records. *Science*, 266,
561 1885–1886, doi.org/10.1126/science.266.5192.1885, 1994.
- 562 Stroeven, A. P., Hättestrand, C., Kleman, J., Heyman, J., Fabel, D., Fredin, O., Goodfellow, B. W., Harbor, J. M.,
563 Jansen, J. D., Olsen, L., Caffee, M. W., Fink, D., Lundqvist, J., Rosqvist, G. C., Strömberg, B. and Jansson,
564 K. N.: Deglaciation of Fennoscandia, *Quat. Sci. Rev.*, 147, 91–121,
565 doi:10.1016/J.QUASCIREV.2015.09.016, 2016.
- 566 Stuiver, M. and Polach, H. A.: Discussion Reporting of ^{14}C Data, *Radiocarbon*, 19(3), 355–363,
567 doi:10.1017/S0033822200003672, 1977.
- 568 Svalgaard, L. and Schatten, K. H.: Reconstruction of the Sunspot Group Number: The Backbone Method, *Sol.*
569 *Phys.*, 291(9–10), 2653–2684, doi:10.1007/s11207-015-0815-8, 2016.
- 570 Svensson, A., Andersen, K. K., Bigler, M., Clausen, H. B., Dahl-Jensen, D., Davies, S. M., Johnsen, S. J.,
571 Muscheler, R., Parrenin, F., Rasmussen, S. O., Röthlisberger, R., Seierstad, I., Steffensen, J. P. and Vinther,
572 B. M.: A 60 000 year Greenland stratigraphic ice core chronology, *Clim. Past*, 4, 47–57, doi.org/10.5194/cp-
573 4-47-2008, 2008.
- 574 van der Plicht, J., van Geel, B., Bohncke, S. J. P., Bos, J. A. A., Blaauw, M., Speranza, A. O. M., Muscheler, R.
575 and Björck, S.: The Preboreal climate reversal and a subsequent solar-forced climate shift, *J. Quat. Sci.*,
576 19(3), 263–269, doi:10.1002/jqs.835, 2004.



577 Vinther, B. M., Clausen, H. B., Johnsen, S. J., Rasmussen, S. O., Andersen, K. K., Buchardt, S. L., Dahl-Jensen,
578 D., Seierstad, I. K., Siggaard-Andersen, M.-L., Steffensen, J. P., Svensson, A., Olsen, J. and Heinemeier, J.:
579 A synchronized dating of three Greenland ice cores throughout the Holocene, *J. Geophys. Res.*, 111(D13),
580 D13102, doi:10.1029/2005JD006921, 2006.

581 Vinther, B. M., Buchardt, S. L., Clausen, H. B., Dahl-Jensen, D., Johnsen, S. J., Fisher, D. A., Koerner, R. M.,
582 Raynaud, D., Lipenkov, V., Andersen, K. K., Blunier, T., Rasmussen, S. O., Steffensen, J. P. and Svensson,
583 A. M.: Holocene thinning of the Greenland ice sheet, *Nature*, 461(7262), 385–388,
584 doi:10.1038/nature08355, 2009.

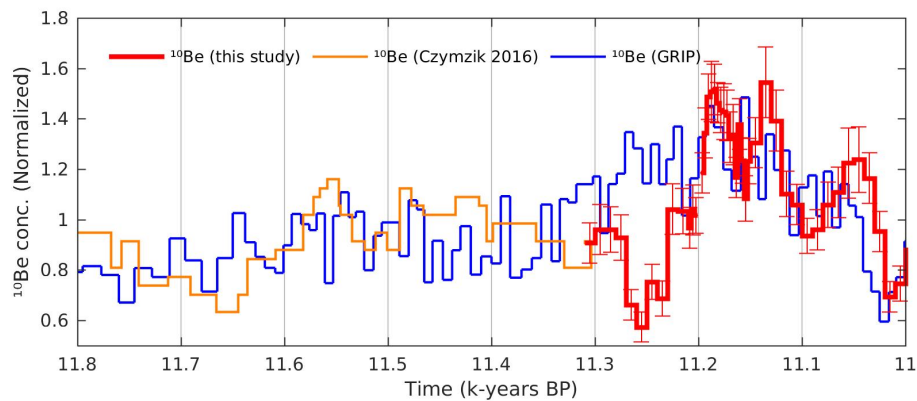
585 von Grafenstein U., Erlenkeuser, H., Brauer, A., Jouzel, J. and Johnsen, S. J.: A mid-european decadal isotope-
586 climate record from 15,500 to 5000 years B.P, *Science*, 284(5420), 1654–7,
587 doi:10.1126/SCIENCE.284.5420.1654, 1999.

588 Vonmoos, M., Beer, J. and Muscheler, R.: Large variations in Holocene solar activity: Constraints from 10 Be in
589 the Greenland Ice Core Project ice core, *J. Geophys. Res.*, 111(A10), A10105, doi:10.1029/2005JA011500,
590 2006.

591 White, J. W. C., Barlow, L. K., Fisher, D., Grootes, P. M., Jouzel, J., Johnsen, S. J., Stuiver, M. and Clausen, H.B.:
592 Stable isotope stacks from GRIP and GISP ice cores, <https://doi.org/10.1594/PANGAEA.716878>, 2009.

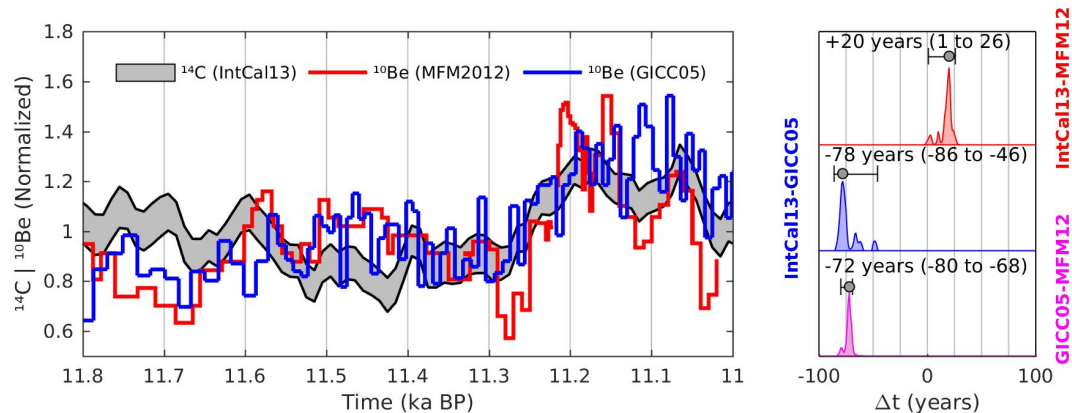
593 Woollings, T., Lockwood, M., Masato, G., Bell, C. and Gray, L.: Enhanced signature of solar variability in
594 Eurasian winter climate, *Geophys. Res. Lett.*, 37(20) doi:10.1029/2010GL044601, 2010.

595
596
597
598
599
600
601
602
603
604
605
606
607
608
609
610
611
612
613
614
615
616
617
618
619
620



621
622
623
624
625
626
627
628
629
630
631
632
633
634
635

Figure 1: The ^{10}Be concentration data from Meerfelder maar (MFM), spanning the period 11,310-11,000 years BP are plotted in red with corresponding measurement error bars. The record is completed in orange with the ^{10}Be measurements from the same sediment profile for the Late Glacial-Holocene transition (Czymzik et al., 2016). The MFM ^{10}Be data are plotted on the original MFM2012 chronology. The ^{10}Be concentration data from the GRIP ice core in central Greenland (Adolphi et al., 2014) is plotted in blue and on the GICC05 time-scale (Rasmussen et al., 2006; Vinther et al., 2006; Svensson et al., 2008; Seierstad et al., 2014). All records have been normalized to their mean.



636

637

638 **Figure 2: Results from the Bayesian wiggle-matching of the different radionuclide records. The left panel shows both the**

639 **MFM ^{10}Be data (in red) and the GRIP ^{10}Be data (blue) once synchronized to the ^{14}C production rate data inferred from the**

640 **IntCal13 calibration curve (1σ grey envelope). The right-hand panel displays the probability density functions for the best**

641 **fit between IntCal13-MFM2012 (in red), IntCal13-GICC05 (in blue) and GICC05-MFM2012 (in magenta), which resulted in**

642 **the synchronization in the left-hand panel and with a 95.4% confidence interval illustrated by the horizontal error bars.**

642



643
644
645
646
647
648
649
650
651
652
653
654
655
656
657
658
659
660
661
662
663
664
665
666
667
668
669
670
671
672
673
674
675
676
677
678
679
680
681
682
683
684
685
686
687
688

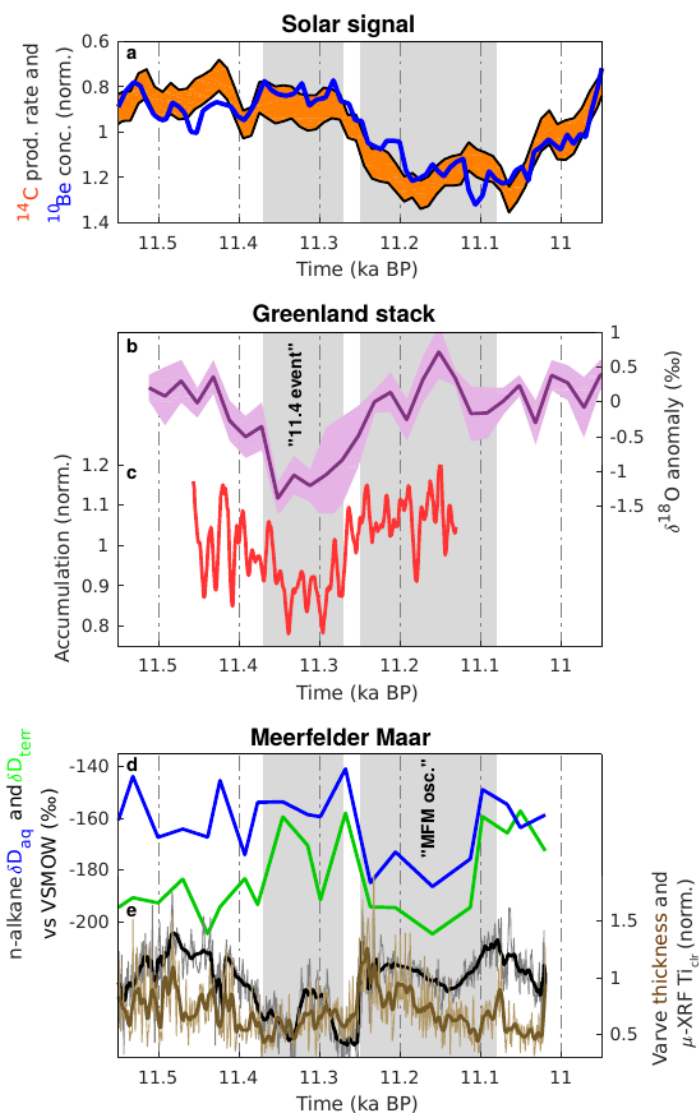
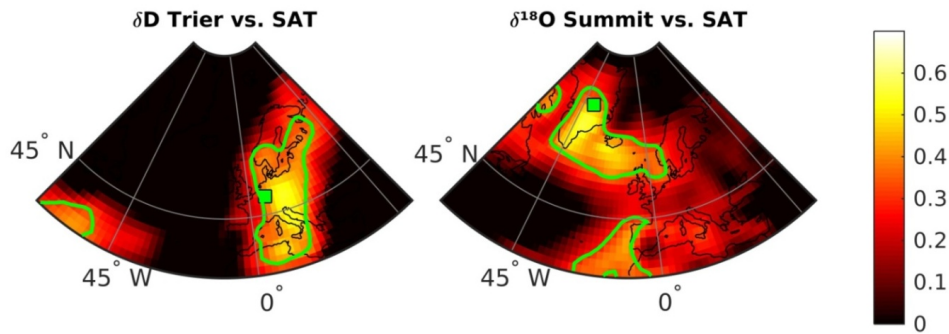


Figure 3: (a) ^{14}C production rate (orange envelope) and GRIP ^{10}Be data (blue) on a reversed y-axis to indicate variations in solar activity. (b) The $\delta^{18}\text{O}$ stack from the DYE-3, GRIP, NGRIP and Renland ice cores (Rasmussen et al., 2007; Vinther et al., 2009) is shown in magenta and (c) the modeled accumulation anomalies from Rasmussen et al. (2007) for DYE-3, GRIP, and NGRIP are shown in red. (d) The δD data record from lipid biomarkers of MFM sediments (Rach et al., 2014) is plotted in blue and green (aquatic and terrestrial) while (e) varve thickness (Martin-Puertas et al., 2012a) and varve $\mu\text{-XRF Ti}_{\text{cr}}$ (Martin-Puertas et al., 2017) are plotted in brown and black, respectively. The grey bands depict the time of occurrence of the 11.4 ka event in Greenland and of the cold oscillation inferred from the MFM sediments (MFM oscillation). All data are plotted on the IntCal13 time-scale, as per Fig. 2.



689
690
691
692
693
694
695
696
697

Figure 4: Left - Correlation map between annual δD in precipitation from the Trier station (green square – IAEA/WMO, 2016) and annual surface air temperatures in the NOAA-CIRES 20th climate reanalysis V2c (Compo et al., 2011) for the period AD 1978-2011. Right – Same as the left panel but for $\delta^{18}O$ from the GISP2 ice core (green square – Steig et al., 1994; White et al., 2009) and for the period AD 1950-1986. Green contour lines represent significance levels for $p < 0.1$ (t-test). The difference in years selected arises from the different time-span of the δD and $\delta^{18}O$ records used here.



698
 699
 700
 701
 702
 703

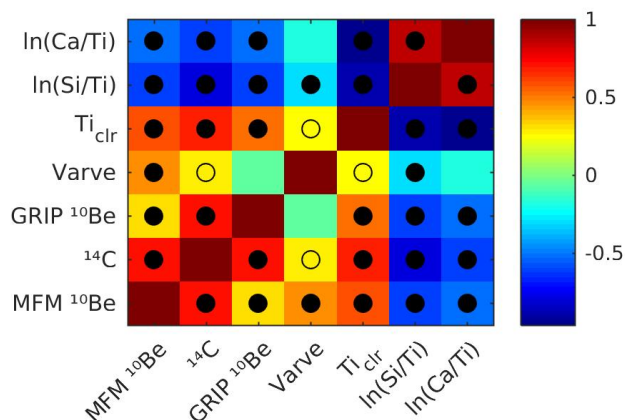
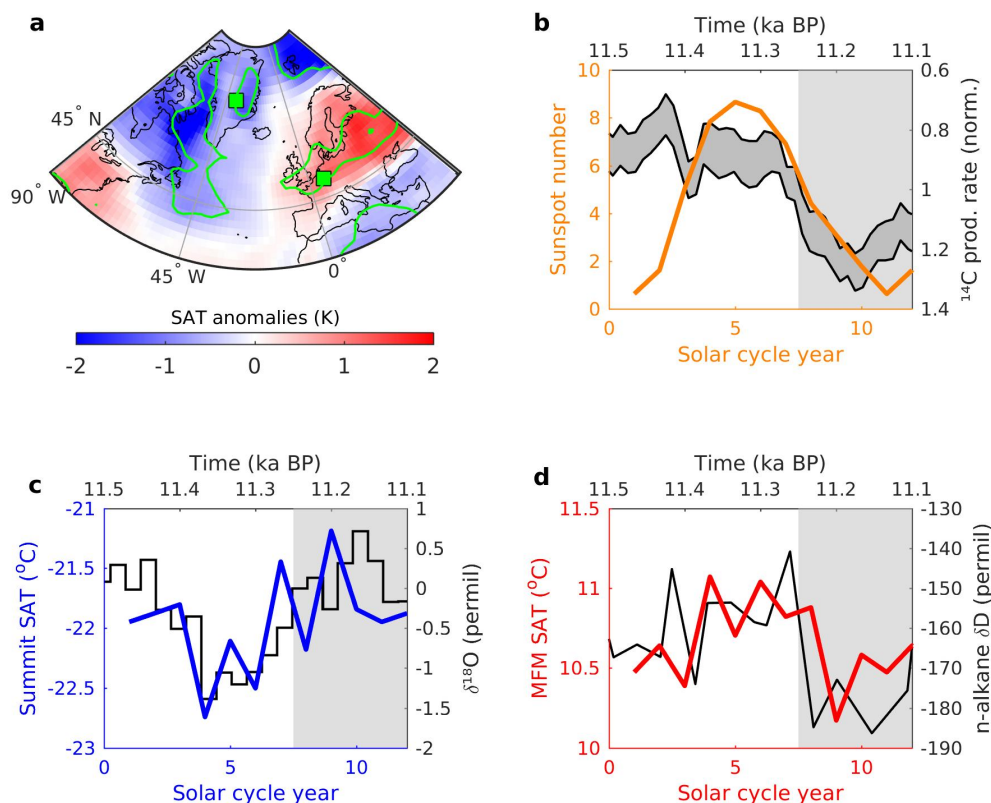


Figure 5: Color-coded correlation matrix between MFM ¹⁰Be concentration, GRIP ¹⁰Be concentration, ¹⁴C production rate data, varve thickness, and μ-XRF data from MFM09 (Martin-Puertas et al., 2017). Open and filled circles denote significant correlations to the p < 0.1 and the p < 0.05 levels, respectively. All data were binned after the resolution of the MFM ¹⁰Be concentration data for the period 11,310-11,000 years BP and a student t-test was performed to test the significance levels.

704
 705
 706
 707

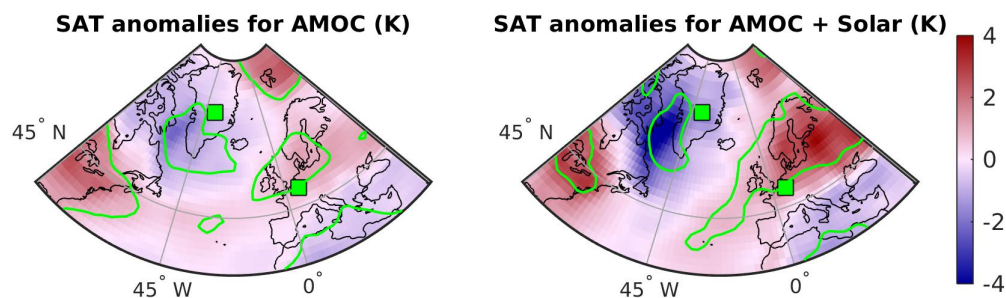


708
 709
 710
 711
 712
 713
 714
 715
 716
 717
 718
 719
 720
 721
 722
 723

Figure 6: The 11.4 ka event and MFM oscillation compared to solar forcing of 20th century SAT in the North Atlantic region, as seen in 20CR. (a) Surface air temperature (SAT) anomalies for solar maxima winters (DJF) compared to solar minima winters (see Sup. Fig. 2) for the period 1946-2011 in 20th century climate reanalysis (Compo et al., 2011). The green squares point to the location of Summit and of MFM while the green contour lines represent significance levels for $p < 0.1$ (t-test). Years influenced by large tropical volcanic eruptions have been removed, as per Ineson et al. (2011). (b) The transition between high to low solar activity in the ^{14}C production rate data (grey envelope - top and right axes) compared to the mean sunspot group number of all 11-year solar cycles during 1900-2011 (orange curve - bottom and left axes). (c) The $\delta^{18}\text{O}$ stack (black curve - top and right axes) shown in Fig. 3b compared to the mean SAT at Summit (blue curve; bottom and left axes) throughout all 11-year solar cycles between 1900-2011 as in (b). (d) Same as (c) but with δD (black curve - top and right axes) and MFM SAT (red curve - bottom and left axes). Note the different time scale on the top (pale records) and bottom axes (reanalysis data). The grey bands show the periods of low solar activity occurring on the two time periods that are compared.



724



725

726

727

728

729

730

Figure 7: Left - Winter (DJF) surface air temperature anomalies for negative AMOC years compared to positive AMOC years for the period 1961-2005 in 20th century climate reanalysis (see Sup. Fig. 4). The green markers point to the location of Summit and of MFM while the green contour lines represent significance levels for $p < 0.1$ (t-test). Right - Same as left panel but for years of both negative AMOC and high solar activity.

731

732

733

734

735

736

737

738

739

740

741

742

743

744

745

746

747

748

749

750

751

752

753

754

755

756

757

758

759

760

761

762